Guided acoustic-wave Brillouin scattering

R. M. Shelby, M. D. Levenson, and P. W. Bayer*
IBM Research Laboratory, San Jose, California 95193
(Received 26 November 1984)

Forward light scattering by the thermally excited guided acoustic modes of an optical fiber produce numerous narrow lines not predicted by the usual theory of Brillouin scattering. Optical heterodyne detection has been used to resolve the scattering spectrum which begins at about 20 MHz and extends to the detection limit. A simple theory quantitatively accounts for the frequencies, polarizations, and intensities of the components. The light scattering from these modes constitutes a thermal-noise source in optical fibers that may prove significant in other experiments.

I. INTRODUCTION

Optical fibers are generally considered passive devices; the light transmitted through them at reasonable power levels may be attenuated, but is not expected to be modulated. Optical fiber sensors utilize the essential passivity of an unperturbed fiber to detect rather small perturbations externally imposed on the fiber.[1] It has long been known, however, that thermally excited vibrational and diffusional fluctuations cause light scattering in glass.[2] This process is responsible for the fundamental limit on the attenuation of light in a fiber, but has not been expected to modulate the transmitted beam for the same reason that a laser beam passing through a glass window is not modulated; scattering in the exact forward direction is possible only at zero-frequency shift. We have, however, detected modulation of the transmitted wave in a single-mode fiber due to thermally excited vibrations. The fact that this effect occurs in a fiber and not in—for example—a long glass laser rod results from the difference between the optical and vibrational modes in the fiber and bulk cases.

A single-mode optical fiber is essentially a long, narrow cylinder of fused silica down the axis of which a single transverse mode of light can propagate, confined by a step in the refractive index.[3] In such a structure, the interaction of light and thermally excited vibrational modes is very different from the bulk scattering described by Mandel'shtam and Brillouin (MB).[4,5] The thermal excitations in a fiber are the eigenmodes of the cylindrical structure rather than the plane waves of the Brillouin theory, and the acousto-optic interaction takes place in a confined geometry that greatly weakens the usual Bragg condition. As a result, the scattered light spectrum consists of dozens of lines, each corresponding to a different cylinder mode rather than the two lines of the MB theory. While light scattering in fused silica has long been studied and the vibrational modes of an elastic cylinder is a classic problem in mechanics, we are the first to our knowledge to detect the resulting fine structure in the light scattering spectrum from an optical fiber.[2,6–9] We have also quantitatively explained the frequencies, polarizations, and intensities of the lines observed for a symmetrical fiber. The presence of this scattered light may have widespread implications in physics and fiber optics.

Previous studies of Brillouin scattering in an optical fiber have concentrated on backwards and right-angle scattering and have employed interferometers of limited resolution.[8] We have concentrated on forward scattering where the scattered wave has the same transverse-mode structure as the incident field and have employed optical heterodyne detection to resolve the fine structure.[10] The Bragg scattering model would predict a zero-frequency shift under these conditions, but since the acoustic modes in a fiber are guided by the cylindrical structure, we find numerous nonzero-frequency shifts in the guided acoustic-wave Brillouin scattering (GAWBS) spectrum between 20 MHz and roughly 800 MHz. The linewidths range down to 50 kHz. Roughly speaking, these modes correspond to the radially and circumferentially propagating acoustical phonons which produce uniaxial strain or dilatation at the core.[7] The resulting oscillatory strain and density fluctuations cause phase and polarization modulation of the confined optical field.

The vibrational modes of a cylinder are characterized by a transverse displacement profile and a wave vector in the direction parallel to the cylinder axis.[6] The transverse profiles can be classified according to the character of their motion as torsional, radial, longitudinal, flexural, or mixtures of these motions. They are assigned mode numbers: n, which give their dependence on the angular coordinate ϕ, and m, which enumerates the modes of each type and corresponds roughly to the number of vibrational nodes within the fiber. The modes responsible for forward scattering light in the core are radial modes independent of ϕ (R_{0m}) or mixed torsional-radial modes varying sinusoidally as 2ϕ (TR_{2m}), the latter being doubly degenerate.[7] A nearly infinite number of modes and a similar number of nonzero mode frequencies exists for each value of the axial wave vector $q_{||}$. This multiplicity of dispersion curves is a key difference between the bulk *MB* scattering case and the present scattering by guided acoustic waves in an optical fiber. The frequencies detected in our experiment correspond to axial wave vectors near

$q_{||}=0$. Only one branch of each of three types of mode—torsional, longitudinal, and flexural—has zero frequency at this point.

II. RESULTS—SYMMETRIC FIBERS

Polarized scattering results from the radial dilatation or R_{0m} modes which cause pure phase modulation. To detect this effect, a single-mode fiber must be used as one arm of a Mach-Zehnder interferometer as in Fig. 1. The other arm of the interferometer transmits the local-oscillator wave necessary for heterodyne detection.[10] The phase fronts, powers, and beam profiles of the two arms are matched on the output beam splitter, and the phase of the local oscillator adjusted to have a component in quadrature with the beam transmitted through the fiber. The interferometer output is detected by a fast-silicon *p-i-n* photodiode, then amplified and dispersed in a radio-frequency spectrum analyzer. The best sensitivity is obtained when the local oscillator also nearly cancels the transmitted intensity. This condition minimizes the average current at the photodiode while maximizing the incident intensity in the fiber.[11] It is important that the shot noise of the detection system be at least 3 dB above the thermal noise. We were able to reach that condition with 5 mW of light on the photodiode and 50 mW of light in the optical fiber. The laser employed was a single axial mode Kr^+ Spectra-Physics model No. 171 laser oscillating at 647 nm. The detector used in the polarized scattering experiments was an EG&G FND-100 high-speed photodiode.

The data reported here was obtained using a 56-cm length of FSV 6000-Å single-mode fiber purchased from Newport Research Corporation. This fiber has a particularly simple internal structure, consisting of a 4.0 ± 0.4 μm diameter core of germania-doped silica surrounded by a 125 ± 3 μm diameter cladding of pure synthetic silica. The external divergence angle of the confined mode was 6.3° at 647 nm. The index of refraction of the core was uniform and 0.003 larger than the cladding.[12] As delivered, the fiber was protected by a jacket of uv-cured acrylate plastic which acted to damp the vibrational modes somewhat and also induced strains and birefringence in the fiber. When the polymer jacket was removed, the residual fiber birefringence was reduced to a few percent and the light scattering spectrum consisted of narrow lines as shown in Fig. 2. Baseline shift due to frequency-dependent amplification was subtracted off digitally. The spectrum clearly shows a rising series of peaks, the spacings of which approach a constant interval at high frequencies. This is consistent with the behavior of the ϕ-independent R_{0m} modes described later.

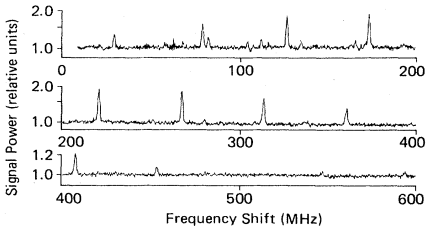

FIG. 2. Polarized guided acoustic-wave Brillouin spectrum from an unjacketed 125-μm nominal diameter single mode optical fiber. The spectrum was obtained using a Mach-Zehnder interferometer and optical heterodyne detection as shown in Fig. 1. The vertical scale is logarithmic, and baseline drift due to the frequency-dependent amplifier response has been subtracted off. The electronic resolution was 1 MHz and the electronic bandwidth of the detection system was 400 MHz. The major peaks correspond to R_{0m} modes and their frequencies appear in Table I. Some minor peaks are due to modes of other symmetry, and some are due to electronic pick up.

The simple apparatus in Fig. 3 suffices to detect depolarized scattering which is due to the TR_{2m} modes. Elliptically polarized light is coupled into the fiber core under conditions where the polarization of the output is identical to the input. We found that a meter or so of unjacketed fiber lying straight on a support fulfilled these conditions. A Glan-Thompson polarizer after the fiber rejects the linear polarization corresponding to the major axis of the input. The much weaker minor-axis polarization is directed onto the photodiode and acts as a local oscillator in heterodyne detection of the depolarized scattering of light initially polarized along the major axis.[11] Figure 4 shows the more complicated spectrum observed for this

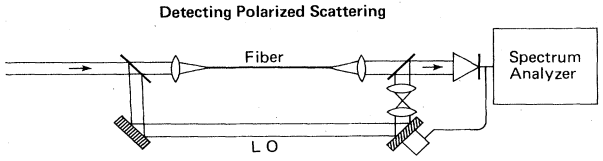

FIG. 1. Apparatus for detecting polarized guided acoustic-wave Brillouin scattering. The device is a Mach-Zehnder interferometer with roughly 1 m of fiber in one arm. The output of the interferometer is collected by an EG&G Corporation FND-100 photodiode. The dc output of the diode is used to control the phase of the reference arm of the interferometer by means of a piezoelectric translator on one mirror. The high-frequency output was amplified and dispersed by an electronic spectrum analyzer. The electronic bandwidth of the system was 400 MHz, and the video averaging bandwidth of the spectrum analyzer was typically 100 Hz.

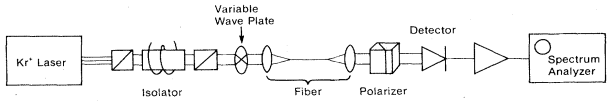

FIG. 3. Apparatus for detecting depolarized guided acoustic-wave Brillouin scattering. The device is an ellipsometer for the fiber with a high-frequency output. The Faraday rotation isolator is needed to prevent reflections from the fiber destabilizing the laser frequency. A variable wave plate similar to a Babinet Soliel compensator produces the correct input polarization to the fiber. The polarizer after the fiber rejects all but a small fraction of the transmitted light. The polarizer output is collected by a Mitsubishi PL-1003 photodiode, the output of which is amplified and dispersed by an electronic spectrum analyzer. The electronic bandwidth of the system was 1 GHz, and most spectra were taken with 300-Hz video bandwidth.

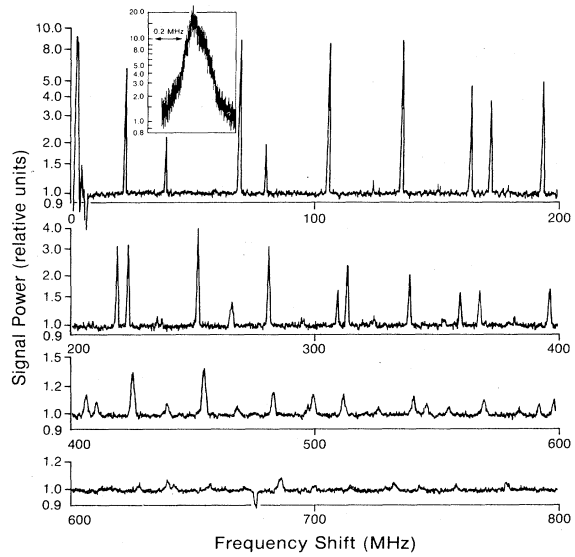

FIG. 4. Depolarized guided acoustic-wave Brillouin spectrum from the 125-μm nominal diameter fiber used for Fig. 1. The polarization spectroscopy technique diagrammed in Fig. 3 was used to provide the local oscillator. The electronic resolution was 0.3 MHz below 400 MHz and 1 MHz above. The electronic bandwidth was 1.0 GHz. The vertical scale is again logarithmic and the amplifier response has been subtracted off. The baseline corresponds to the shot noise level with 5 mW on the detector. The frequencies of the major components appear in Table I and agree with calculated TR_{2m} mode frequencies. The inset shows the 104.6-MHz mode at a resolution of 10 kHz. The deviation from a Lorentzian line shape results from small variations in the fiber diameter.

polarization when the power coupled into the fiber core was 200 mW and the power at the detector was 1–5 mW.

The inset of Fig. 4 shows one of the stronger lines, which has a characteristic near-Lorentzian line shape. By normalizing the power scattered by this mode in the forward direction to the shot-noise power at the baseline, one can calculate the scattering efficiency per unit length.[11] The experimental forward scattering efficiency is $\eta_F=(1.2\pm0.4)\times10^{-12}$ cm^{-1}. This is roughly two orders of magnitude less than the efficiency of depolarized Brillouin scattering at 90° in bulk fused silica but as there are roughly 30 strong modes present in a fiber, the total scattering efficiency is comparable to the bulk case.[2]

We found that the presence or absence of a polymer fiber jacket did not measurably alter the frequencies of the cylinder-guided acoustic waves but did greatly alter the linewidths observed in our spectra. This is to be expected since the polymer jacket tends to dampen vibrations at the circumference of the silica fiber. The linewidth of the mode shown in the inset was 165 kHz full width at half maximum (FWHM) in the unjacketed fiber and 1000 kHz in an identical jacketed fiber.

III. THEORY AND DISCUSSION

The theory of the vibrational modes of a long cylinder has been reviewed by Thurston and Sittig and Coquin.[6,7] In a uniform cylinder, the frequencies of these modes depend only upon the cylinder radius a, the velocity of longitudinal (dilatation) waves V_d, the velocity of transverse (shear) waves V_s, and the wave vector along the cylinder axis $q_{||}$. Our scattering is due to modes with $q_{||}=0$. All branches of both R_{0m} and TR_{2m} series of modes have nonzero frequency and little dispersion around $q_{||}=0$. Each mode couples the incident and a forward scattered photon thus giving a Stokes and anti-Stokes peak in the light scattering spectrum for each mode, each of which contributes to the amplitude of the single beat frequency detected by the spectrum analyzer. The phase velocity for these waves approaches infinity for $q_{||}\sim0$, while the group velocity approaches zero. The transverse spatial dependence of the modes and their resonant frequencies can be determined by solving the differential equations with the appropriate boundary conditions, and the radial dependence of the displacements can be expressed in terms of Bessel functions, $J_n(z)$.

For the dilatational R_{0m} modes, the boundary condition corresponding to the free fiber surface can be written as

$$(1-\alpha^2)J_0(y)-\alpha^2J_2(y)=0\ , \tag{1}$$

where $\Omega_m=(V_dy_m)/a$ gives the frequency of the mth mode, $\alpha=V_s/V_d$, and y_m is the mth zero of Eq. (1).[6,7] For fused silica, $V_s=3740$ m/sec and $V_d=5996$ m/sec.[8] For our nominal fiber radius of $a=62.5$ μm,[12] we calculate $V_d/2\pi a=15.3$ MHz, and $\alpha=0.62$. The best fit to experimental spectra was obtained for $\alpha=0.6203$ and $V_d/2\pi a=14.801$ MHz, leading to the calculated mode frequencies in Table I.

The displacement of a point within the fiber by these modes can be expressed in cylindrical coordinates as

$$U_{rm}(r)=C_{Rm}J_1\left[y_m\frac{r}{a}\right],\quad U_{\phi m}=U_{zm}=0 \tag{2}$$

where C_{Rm} is amplitude of a thermally excited low-frequency vibration calculated from the equipartition theorem.[2] The total vibrational energy for a single mode in a fiber of length l and density ρ is

$$E_m=\int_0^l\int_0^{2\pi}\int_0^a\tfrac{1}{2}\rho\Omega_m^2[U_{rm}^2(r)+U_{\phi m}^2(r)]r\,dr\,d\theta\,dz\ , \tag{3}$$

which must equal kT. For each R_{0m} mode, the thermally excited amplitude is then

$$C_{Rm}=\left[\frac{kT}{\pi l\rho\Omega_m^2a^2B_{Rm}}\right]^{1/2}, \tag{4}$$

where

$$B_{Rm}=\int_0^1J_1^2(y_mx)x\,dx \tag{5}$$

is the required radial integral.

The light scattering efficiency can be calculated from the radial and azimuthal strain at the core using the known strain-optic coefficients of fused silica. For $q_{||}=0$ modes, the nonvanishing strain components are

TABLE I. Observed polarized and depolarized scattering frequencies compared to calculated R_{0m} and TR_{2m} frequencies for $a=64.47$ μm; $V_s/V_d=0.6203$ and $V_d=5996.0$ m/s.

Polarized frequencies		Depolarized frequencies					
Observed (MHz)	Calculated R_{0m} (MHz)	Observed (MHz)	Calculated TR_{2m} (MHz)	Observed (MHz)	Calculated TR_{2m} (MHz)	Observed (MHz)	Calculated TR_{2m} (MHz)
29.72	29.67	21.52	21.52	405.76	406.50		684.53
79.62	79.57	38.20	38.15	410.26		685.52	685.85
127.20	126.75	68.41	68.41	425.05	425.05	699.11	
135.13	TR_{2m}	79.23	78.89	439.32			713.62
173.44	173.56	104.58	104.58		452.59	731.97	732.13
220.32	220.23		122.88	454.32	454.30		742.49
267.31	266.84	135.14	134.97	468.41			771.30
313.68	313.87	163.41	163.27	482.72	482.75	778.54	778.68
360.47	360.37	171.57	171.41	499.24	499.53		800.18
407.29	406.87	192.97	193.81	511.62	511.66	825.21	825.13
453.60	453.37	218.23	217.80	540.23	540.43		829.07
	499.87	222.66	223.31	545.56	546.13		857.87
546.69	546.37	251.33	251.60	555.07		872.16	871.68
592.77	592.87	265.50	265.22	569.61	569.35		886.73
	·	280.39	280.67	583.50			915.52
	·	308.72	309.24	591.99	592.54	918.77	918.24
	·	312.81	313.61	598.51	598.26		944.42
		338.32	338.40	627.43	627.04	964.91	964.69
		359.15	359.82	638.93	639.12		973.28
		367.27	367.39	641.44			1002.11
		396.21	396.11	656.06	655.92		1011.21
							⋮

$$S_{rr}=\frac{\partial U_r}{\partial r}\ ,$$
$$S_{\phi\phi}=\frac{U_r}{r}+\frac{1}{r}\frac{\partial U_\phi}{\partial \phi}\ , \tag{6}$$
$$S_{r\phi}=\frac{1}{r}\frac{\partial U_r}{\partial \phi}+\frac{\partial U_\phi}{\partial r}-\frac{U_\phi}{r}\ .$$

For the R_{0m} modes the nonvanishing strain components become

$$S_{rr}=C_{Rm}\left[\frac{1}{r}J_1\left[\frac{y_m r}{a}\right]-\frac{y_m}{a}J_2\left[\frac{y_m r}{a}\right]\right]\ ,$$
$$S_{\phi\phi}=C_{Rm}\frac{1}{r}J_1\left[\frac{y_m r}{a}\right]\ . \tag{7}$$

The resulting scalar change in the index of refraction at a point at radius r inside the fiber is

$$\Delta n(r)=\frac{n^3(P_{11}+P_{12})}{2}[S_{rr}(r)+S_{\phi\phi}(r)]\ , \tag{8}$$

where $P_{11}=0.121$ and $P_{12}=0.270$ are the strain-optic coefficients for fused quartz[13] and n is the refractive index. The phase shift of the light propagating down the core can be estimated by averaging the refractive index perturbation $\Delta n(r)$ over the mode profile of the guided optical wave $E(r)\approx(1/\pi w^2)e^{-(r/w)^2}$:

$$\epsilon=\frac{2\pi\omega l}{c}\int_0^a \Delta n(r)E(r)r\,dr\ , \tag{9}$$

where the mode radius w can be estimated from the divergence angle or the core radius. Phase-modulation theory then implies that two sidebands are created, shifted by the vibrational mode frequency $\pm\Omega_m$, and that the forward scattering efficiency for each sideband is

$$\eta_F=\left[\frac{J_1(\epsilon)}{J_0(\epsilon)}\right]^2 l^{-1}\approx\left[\frac{\epsilon}{2}\right]^2 l^{-1}\ , \tag{10}$$

where the inverse of the fiber length l is required for dimensional consistency.[14] The profile of the guided optical mode can be approximated by a Gaussian function with a mode radius w roughly 30 times less than the radius of the fiber a. The Bessel functions in Eq. (7) can then be approximated by their lowest nonvanishing term in r for modes which satisfy the condition $y_m/\pi \ll a/w$. This holds for the first ten or so R_{0m} modes. The index perturbation and scattering efficiency then become

$$\Delta n(r)=\frac{n^3(P_{11}+P_{12})C_{Rm}y_m}{4a}\ , \tag{11}$$
$$\eta_F=\frac{n^6\omega^2 kT(P_{11}+P_{12})^2}{32\pi c^2\rho V_d^2 a^2 B_{Rm}}\ . \tag{12}$$

For the strong polarized R_{0m} mode at 127 MHz, these calculations imply a total forward scattering efficiency $\eta_F=4.4\times10^{-12}$ cm^{-1}, in approximate agreement with the value implied by our observations.

The depolarized TR_{2m} modes are more complex. The boundary condition of zero traction at the fiber surface implies the characteristic equation:

$$\begin{vmatrix} [(3-y^2/2)J_2(\alpha y)] & [(6-y^2/2)J_2(y)-3yJ_3(y)] \\ [J_2(\alpha y)-\alpha y J_3(\alpha y)] & [(2-y^2/2)J_2(y)+yJ_3(y)] \end{vmatrix}=0 , \tag{13}$$

where the mode frequencies are $\Omega_m = V_s y_m / a$.[6,7] The results appear in Table I. Clearly, the agreement with the measured mode frequencies is excellent for both polarized and depolarized modes. The TR_{2m} modes are doubly degenerate; the isoclines can be at 0° and 90° or at ±45°. The displacements corresponding to the 0°–90° modes are

$$U_r(r,\phi)=C_{Tm}u_r(r/a)\cos(2\phi) ,$$
$$U_\phi(r,\phi)=C_{Tm}u_\phi(r/a)\sin(2\phi) , \tag{14a}$$

where

$$u_r(r/a)=A_1\frac{2}{(r/a)}J_2\left[\frac{y_m r}{a}\right]-A_2\left[\frac{2}{(r/a)}J_2\left[\frac{\alpha y_m r}{a}\right]-\alpha y_m J_3\left[\frac{\alpha y_m r}{a}\right]\right]$$
$$u_\phi(r/a)=A_2\frac{2}{(r/a)}J_2\left[\frac{\alpha y_m r}{a}\right]-A_1\left[\frac{2}{(r/a)}J_2\left[\frac{y_m r}{a}\right]-y_m J_3\left[\frac{y_m r}{a}\right]\right] , \tag{14b}$$

with

$$A_1=(6-y_m^2)J_2(\alpha y_m) ,$$
$$A_2=(6-y_m^2/2)J_2(y_m)-3y_m J_3(y_m) . \tag{14c}$$

The amplitudes corresponding to thermal excitation can again be calculated from Eq. (3):

$$C_{Tm}=\left[\frac{2kT}{\pi l\rho\Omega_m^2 a^2 T_m}\right]^{1/2} , \tag{15}$$

where the relevant radial integral is

$$T_m=\int_0^1\{[u_r(z)]^2+[u_\phi(z)]^2\}z\,dz . \tag{16}$$

All three elements of the strain tensor given in Eq. (6) are nonzero for the TR_{2m} modes:

$$S_{rr}=\frac{C_{Tm}}{a}\left\{A_2\left[\frac{-2}{(r/a)^2}J_2\left[\frac{\alpha y_m r}{a}\right]+\frac{5\alpha y_m}{(r/a)}J_3\left[\frac{\alpha y_m r}{a}\right]+(\alpha y_m)^2 J_4\left[\frac{\alpha y_m r}{a}\right]\right]\right.$$
$$\left.+A_1\left[\frac{2}{(r/a)^2}J_2\left[\frac{y_m r}{a}\right]-\frac{2y_m}{(r/a)}J_3\left[\frac{y_m r}{a}\right]\right]\right\}\cos(2\phi) , \tag{17a}$$

$$S_{\phi\phi}=\frac{C_{Tm}}{a}\left\{A_2\left[\frac{2}{(r/a)^2}J_2\left[\frac{\alpha y_m r}{a}\right]+\frac{\alpha y_m}{(r/a)}J_3\left[\frac{\alpha y_m r}{a}\right]\right]\right.$$
$$\left.+A_1\left[\frac{-2}{(r/a)^2}J_2\left[\frac{y_m r}{a}\right]+\frac{y_m}{(r/a)}J_3\left[\frac{y_m r}{a}\right]\right]\right\}\cos(2\phi) , \tag{17b}$$

$$S_{\phi r}=\frac{C_{Tm}}{a}\left\{A_2\left[\frac{4}{(r/a)^2}J_2\left[\frac{\alpha y_m r}{a}\right]-\frac{4\alpha y_m}{(r/a)}J_3\left[\frac{\alpha y_m r}{a}\right]\right]\right.$$
$$\left.+A_1\left[\frac{-4}{(r/a)^2}J_2\left[\frac{y_m r}{a}\right]+\frac{4y_m}{(r/a)}J_3\left[\frac{y_m r}{a}\right]-y_m^2 J_4\left[\frac{y_m r}{a}\right]\right]\right\}\sin(2\phi) . \tag{17c}$$

The calculation of the polarization and phase shift of the light propagating down the core is very similar to, but more complex than, that for the R_{0m} modes. Approximating the Bessel functions by their small r expansions results in a major simplification which is again appropriate for $y_m/\pi \ll a/w$. The leading terms in the anisotropic index of refraction perturbation are then

$$\Delta n_\perp=\frac{n^3}{2}\frac{C_{Tm}}{a}\left[\frac{y_m}{2}\right]^2(A_1-\alpha^2 A_2)(P_{11}-P_{12}) . \tag{18}$$

Light propagating with linear polarization at $\phi=45°$ encounters anisotropic perturbations which cause unequal phase shifts for components projected on the $\phi=0°$ and $\phi=90°$ axes. Polarization components are created along $\phi=-45°$ that are frequency up shifted and down shifted by the vibrational mode.[15] The fraction depolarized in this way by the index perturbations is

$$\eta_F=\frac{n^6\omega^2 kT(A_1-\alpha^2 A_2)^2(P_{11}-P_{12})^2}{64\pi c^2\rho V_s^2 a^2 T_m} . \tag{19}$$

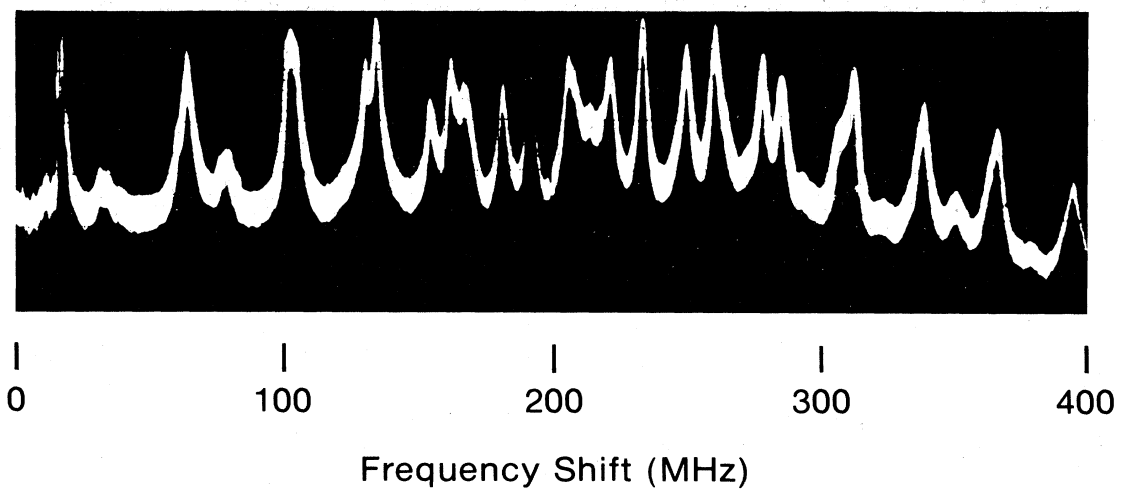

FIG. 5. Depolarized GAWBS spectrum of an Hitachi 6315 fiber complete with polymer jacket. The overall vertical scale is 12 dB, the resolution is 300 kHz and the video bandwidth 300 Hz.

For the TR_{25} mode at 105 MHz, Eq. (19) predicts a scattering efficiency of 1.4×10^{-12} cm^{-1} for forward scattering in satisfactory agreement with our measured value of $(1.2\pm0.4)\times10^{-12}$ cm^{-1}. Equation (19) also correctly predicts the pattern of relative peak intensities in Fig. 4.

The modes with frequency shifts above roughly 300 MHz do not fulfill our $y_m/\pi \ll a/w$ condition. The radial dependence of the index of refraction perturbation of these modes varies across the core. When $y_m w/a \approx \pi$, a node will exist within the region sampled by the transmitted light beam, giving rise to a partial cancellation of the phase shifting effect of the vibration. One should note that the scattering efficiencies of Eqs. (12) and (19) increase roughly as Ω_m until this cancellation occurs. Beyond that point, one would expect that the light scattering due to high-frequency modes would drop off with increasing frequency, and such is the observed result. Even so, thermally excited guided acoustic-wave scattering is observed up to the maximum frequency of our detection system, and the frequencies of most of these modes can be accounted for by our theory. One would expect that the different acoustical parameters of the core material and the effects of strain and other inhomogeneities in the cladding structure would perturb individual high-frequency modes in characteristic ways. Low-frequency modes, on the other hand, would be perturbed less and more uniformly because the characteristic radii of the core and the perturbations are then smaller than the radii of the nodes. While we have detected perturbations of this sort, we have made no attempt to explain them quantitatively. Modes with nodes inside the core region would also tend to scatter light out of the guided optical mode, further reducing the detected heterodyne signal.

IV. RESULTS—NONAXISYMMETRIC FIBERS

We have also studied symmetrical fibers with overall diameter different than the FSV fiber and fibers with elliptical cores or nonaxisymmetric stress patterns which preserve polarization.[16–18] The symmetric fibers show scattering spectra similar to Figs. 2 and 4 but with the frequency scale altered by the ratio of fiber diameters. Fibers with aluminum metal jackets show somewhat more complex patterns because of the good acoustical coupling between the silica fiber and the jacket.[18]

The nonaxisymmetric fibers show considerably more complex scattering spectra. Figure 5 shows the depolarized spectrum of the Hitachi 6315 fiber as it is delivered. This fiber has the same overall diameter as the FSV fiber, but the polymer jacket damps the vibrational modes quite well, leading to the large linewidths observed. Within the frequency precision possible with such linewidths, there is little difference between the modes of such a fiber and the FSV fiber. Figures 6 and 7 show the polarized and depolarized spectra of an Hitachi 6315 fiber from which the polymer jacket has been removed. At low frequencies, the patterns are quite similar to Figs. 2 and 4, but fine splittings can be observed in the depolarized spectrum beginning at about 100 MHz.

The TR_{2m} modes in a symmetric fiber are doubly degenerate; the vibration patterns of the two degenerate modes are rotated by 45° with respect to one another. The nonsymmetric strain patterns caused by the structure and

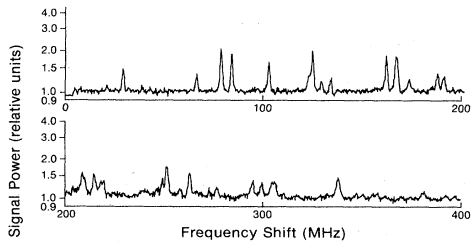

FIG. 6. Polarized GAWBS spectrum from an Hitachi 6315 fiber without its polymer jacket. The conditions are similar to those in Fig. 2, and the differences in the spectra reflect the differences in fiber structures. The resolution is 1 MHz.

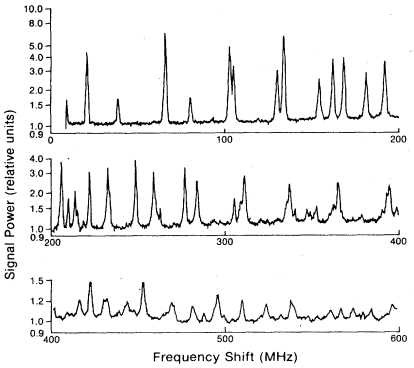

FIG. 7. Depolarized GAWBS spectrum from an unjacketed Hitachi 6315 fiber with the incident polarization along the fast or slow axis of the fiber. The spectrum is similar to that in Fig. 4; the differences reflect the more complex internal structure of this fiber which has an elliptical region in the cladding with a different composition. The resolution is 1 MHz.

composition of the cladding of a polarization preserving fiber and the noncylindrical interfaces within the cladding lifts this degeneracy, introduces a new splitting and creates a polarization selection rule. The GAWBS modes which scatter light from the fast to the slow polarization directions (and vice versa) create strain at the core at an angle of 45° to the fast and slow polarizations. These modes are one of the two sets of TR_{2m} modes of the fiber. The other set creates strain along the linear polarization directions and thus cannot be detected by polarization techniques when the incident light propagating through the fiber remains linearly polarized. If, however, the polarization incident on the fiber excites both the fast and slow modes equally, the light polarization within the fiber will oscillate between linear, circular, and elliptical states. The linear polarization, for example, will be at 45° to the strain direction of the second set of TR_{2m} modes, and thus can be depolarized by these vibrations. Similar considerations apply to the other polarization states occurring at other locations in the fiber.

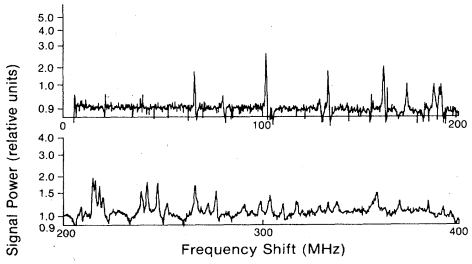

FIG. 8. Additional depolarized GAWBS peaks that appear when the incident polarization has both fast and slow components. The spectrum was obtained by digitally subtracting traces similar to Fig. 7 from corresponding traces taken in the other polarization condition. Some of the high-frequency peaks seem related to polarized GAWBS modes. Resolution is 300 kHz for frequencies below 200 MHz, 1 MHz above.

To detect this second set of TR_{2m} modes, one thus must excite the fast and slow polarizations of the fiber equally with the incident light, and use a variable wave plate and polarizer to reject a large fraction of the transmitted light. This light will be in some elliptical polarization at the output end of the fiber, but will remain constant if the temperature or strain of the fiber does not vary. The light transmitted by the polarizer is again incident upon a photodiode and the beating signals dispersed by the spectrum analyzer. The resulting spectrum is similar to Fig. 7, containing peaks due to both sets of TR_{2m} modes. Our spectrum analyzer allows digital subtraction of one spectrum from another. The peaks that appear only when the incident radiation propagates in both the fast and slow modes remain after the subtraction. Such a difference spectrum appears in Fig. 8. The fact that fewer peaks appear in this trace than in Fig. 7 indicates that the splittings of the two sets of TR_{2m} modes are small for most modes of the Hitachi 6315 fiber.

The fine structure of the depolarized GAWBS spectrum of this fiber is better illustrated in Fig. 9, which shows the region of TR_{25} modes. With the incident radiation mostly in the fast polarization in the fiber, and the detected light in the slow polarization, the two peaks in the top trace of Fig. 9 appear. When the incident and detected polarizations were shifted to excite one linear combination of fast and slow and to detect the orthogonal combination, the additional peaks in the bottom trace of

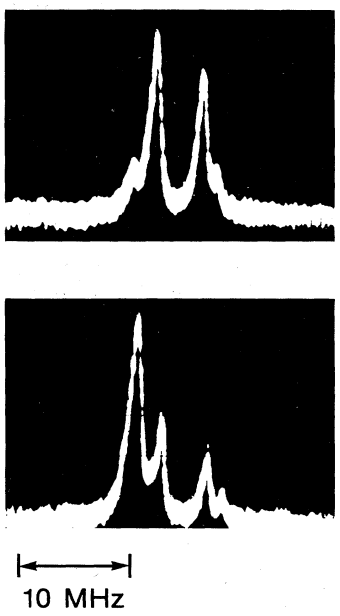

FIG. 9. Variation in the TR_{25} components due to the polarization selection rule in Hitachi 6315 fiber. The top figure shows the peaks appearing near 103 MHz when the incident light was mostly polarized along one fiber axis. The lower trace shows the same region when the incident light has mixed polarization. The two outermost peaks have increased in intensity with respect to the two inner peaks. The resolution was 300 kHz, the video bandwidth was 300 Hz, and the overall vertical scale 12 dB for each figure.

TABLE II. Polarized scattering frequencies for Hitachi 6315 fiber (MHz).

29.05	132.8	214.6	304.4
65.79	160.9	218.0	337.3
77.80	166.3	251.2	380.8
83.15	172.8	262.9	391.4
101.8	186.6	276.5	396.3
123.9	189.9	293.6	
128.7	208.6	298.6	

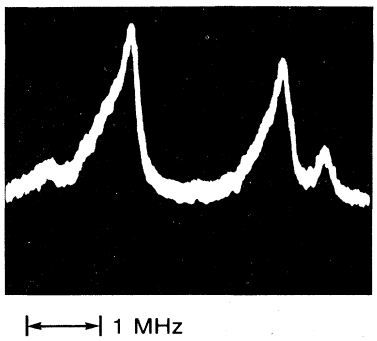

FIG. 10. Line shapes of the TR_{25} components seen with near linear polarized incident light. The triangular line shape is characteristic of this fiber. The vertical scale is again 12 dB overall, the resolution was 30 kHz, and the video bandwidth was 10 Hz.

Fig. 9 appeared. The line shapes of the individual modes are not symmetric in this fiber, but have longer wings on the low-frequency side. Figure 10 shows the two frequency components of the TR_{25} mode accessed with linear polarization. A similar trace with a baseline produced by a tungsten light yielding the same electronic current showed that the noise level fell to the shot noise level away from the peaks when the optical power at the detector was 5 mW.

Birefringent fibers support two orthogonally polarized optical modes with different phase velocities, called the slow and fast modes. Scattering from one to the other requires a wave-vector change $\Delta k_0=(n_s-n_f)\omega/c=\pi/l_B$ even when no frequency shift occurs. The effective indices of refraction for the fast and slow waves are n_f and n_s, respectively, and parameter l_b is the beat length of the fiber which equals 5 mm for the Hitachi 6315. If the scattering from the fast to the slow modes is due to guided acoustic waves, the axial wave vector of the acoustic mode must be nonzero for such fibers. Away from $q_{||}=0$, the dispersion curves for the guided acoustic modes need not be flat. The scattered frequency is slightly larger than that at zero wave vector. The GAWBS wave at wave vector q has frequency

$$\Omega=\Omega_0+\mu q^2 ,$$

where the parameter μ defines the curvature of the dispersion curve at zero wave vector. Thus the frequency shift in the scattered light has magnitude

$$\Omega=\Omega_0+\mu\Delta k_0^2 .$$

The asymmetries in the Hitachi 6315 fiber also couple modes of different symmetry to one another and further complicate the light scattering spectra, especially at large frequency shift. We have not attempted to analyze the observed peak frequencies, but we have measured them quite accurately using the frequency counter in our spectrum analyzer. The frequencies of the polarized modes and the modes responsible for depolarized scattering of fast or slow wave incident light appear in Tables II and III. Table IV shows the additional peaks that appear in the depolarized spectrum when the incident light has mixed polarization.

There are now a wide variety of designs for polarization preserving fibers, and we expect that the details of the GAWBS spectra will be different for each type of fiber. These differences may not be observable for fibers with highly damping polymer jackets, but should appear when the jacket is removed. It may be possible to use these spectra to analyze the internal structure of an unknown fiber once a sufficient theoretical understanding of the perturbations has been developed.

V. CONCLUSION

In conclusion, we have shown that thermally excited guided acoustic modes cause phase modulation and depolarization of light guided by a single-mode optical fiber. The resultant light scattering can be detected by optical heterodyne techniques in forward scattering, and the frequency shifts of the scattered light are in quantitative agreement with a simple theory. The observed intensities appear consistent with the predictions of our thermal ex-

TABLE III. Depolarized scattering frequencies for Hitachi 6315 fiber with a linear polarized incident wave (MHz).

20.38	162.33	232.8	337.3	398.1	479.3
38.79	168.55	249.3	340.2	400.6	485.8
66.59	181.30	259.7	347.5	415.1	493.9
80.64	191.9	263.4	352.7	421.3	508.0
102.99	205.7	277.5	362.3	428.7	522.5
105.31	209.5	284.3	365.2	430.5	538.4
130.43	213.4	305.4	378.5	442.1	559.0
134.38	214.8	309.7	392.8	451.4	565.4
154.39	221.8	311.3	394.1	467.23	572.4

TABLE IV. Depolarized scattering peaks occurring only for mixed incident polarization for the Hitachi 6315 fiber (MHz).

65.73	161.2	208.6	238.4	272.3	310.0	357.7
79.61	172.7	214.7	241.4	276.3	317.2	369.3
101.9	186.9	215.6	246.7	290.7	329.1	384.7
129.8	189.7	217.4	251.2	298.6	333.3	392.1
133.3	190.5	219.3	265.1	304.2	337.4	395.8

citation model. The linewidths of the various frequency components increase with frequency and are dependent on the acoustical characteristics of the material used to sheathe the silica fiber. While this study has focused on modes with near-zero wave vector along the fiber axis, corresponding modes exist with nonzero axial wave vector, and these too should be capable of scattering light. In particular, modes with $q_{\|}=4\pi n/\lambda$ cause backscattering of the incident radiation with a frequency shift of $\Omega_m \approx 4\pi n V_d/\lambda$. The linewidth of the observed backward Brillouin scattering is roughly 145 MHz in a fiber, which is less than the splitting observed here.[8,18] On the basis of our analysis, one would predict that a pattern of splittings similar to that reported here should be detectable in the backscattering case.

This light scattering phenomenon constitutes a thermal-noise source within all optical fibers and might ultimately be significant in communications and sensor applications of these devices. In particular, attempts to use optical fibers to generate or transmit squeezed states of radiation must avoid conditions where the thermal noise due to these guided acoustic waves exceeds the residual quantum noise.[19] The noise source is quite weak; even with a scattering efficiency of 4.4×10^{-12} cm^{-1} for a 100-MHz mode and a scattering efficiency that increases with mode frequency for 30 or so modes, the total noise power produced by a kilometer of fiber is only 6.6×10^{-5} of the transmitted power. The loss in such a fiber is 96% of the incident power. Averaged over the bandwidth of the fiber, the fractional noise level is 1×10^{-14} Hz^{-1}km^{-1}. Even so, this noise source must be considered carefully in the design of optically heterodyne detected fiber optic systems, especially if an optical fiber is to be used to transmit the local oscillator to a detector.

ACKNOWLEDGMENTS

The authors acknowledge helpful conversations and material assistance from Dr. Roger Stolen and Professor George Stegeman, and the technical assistance of Michael Trump. This project has been partly supported by the Office of Naval Research.

*Present address: Fairchild Advanced Research and Development Laboratory, 4001 Miranda Ave., Palo Alto, CA 94304.

[1]T. G. Giallorenzi, J. A. Bucaro, A. Dandridge, G. H. Sigel, Jr., J. H. Cole, S. C. Rashleigh, and R. G. Priest, IEEE J. Quantum Electron. **QE-18**, 626 (1982).

[2]I. L. Fabelinsky, *Molecular Scattering of Light* (Plenum, New York, 1958), Chap. VII.

[3]L. B. Jeunhomme, *Single Mode Fiber Optics* (Marcel Dekker, New York, 1983).

[4]L. I. Mandel'shtam, Zh. Russ. Fiz. Khim. Obshchestva **58**, 381 (1926).

[5]L. Brillouin, Ann. Phys. (Paris) **17**, 88 (1922).

[6]R. N. Thurston, J. Acoust. Soc. Am. **64**, 1 (1978).

[7]E. K. Sittig and G. A. Coquin, J. Acoust. Soc. Am. **48**, 1150 (1970).

[8]P. T. Thomas, N. L. Rockwell, H. M. van Driel, and G. I. Stegeman, Phys. Rev. B **19**, 4986 (1979).

[9]M. D. Levenson, R. M. Shelby, and P. W. Bayer, Phys. Rev. Lett. **54**, 939 (1985).

[10]D. Marcuse, *Engineering Quantum Electronics* (Harcourt, Brace, and World, New York, 1971), Chap. 6.

[11]M. D. Levenson and G. L. Eesley, Appl. Phys. **19**, 1 (1979).

[12]Light Wave Technology, Inc., data sheet for type F1506C fiber (1983).

[13]R. W. Dixon, J. Appl. Phys. **38**, 5149 (1967).

[14]A. Yariv, *Quantum Electronics* (Wiley, New York, 1975), Chap. 14.4.

[15]J. C. Kemp, J. Opt. Soc. Am. **59**, 950 (1969).

[16]R. B. Dyott, J. R. Cozens, and D. G. Morris, Electron. Lett. **15**, 380 (1974).

[17]Hitachi Corporation, SP-6315 single polarization fiber data sheet F4-911C (1983).

[18]E. P. Ippen and R. H. Stolen, Appl. Phys. Lett. **21**, 539 (1972).

[19]D. F. Walls, Nature **306**, 141 (1983).